HEFAT2014
10th International Conference on Heat Transfer, Fluid Mechanics and Thermodynamics
14 – 16 July 2014
Orlando, Florida

COMPARISONS BETWEEN DYNAMICS OF SBSL AND AN ENCAPSULATED BUBBLE IN SPHERICAL RESONATOR

[1]M. Navarrete*, [2]S. Cruz, [3]F. Castellanos, [2]J.L. Naude, and [2]F. Méndez
*Author for correspondence
[1]Instituto de Ingeniería, Universidad Nacional Autónoma de México, D. F.,
[2]Facultad de Ingeniería, Universidad Nacional Autónoma de México, D. F.,
Av. Universidad 3000,
[3]Instituto Politécnico Nacional, IPN, CIIDIR, Oaxaca,
México,
E-mail: mnm@pumas.iingen.unam.mx

ABSTRACT

Single bubble sonoluminescence (SBSL) and ultrasound agent contrast (UAC), each one levitating in a standing wave field (30~70 kHz) inside of a spherical resonator filled with sterile water, are compared in order to understand their radial dynamics. Light scattering technique is employed to measure the radial pulsations of individual/cloud microbubbles. Waves emitted by bubble (shock wave) and the intensity of the acoustic field applied are measured through a needle hydrophone. UAC is highly diluted Polyson® microbubbles. Waveforms are processed by means of Fourier and time-frequency analysis. The experimental data and the main parameters involved (T, ρ, Pa, Re and De) are analyzed as a function of short and long regimen. Linear and nonlinear oscillations were observed and associated with time-frequency spectra. Parametric instabilities are inferred from the light-scattered signal. The resting diameter and temperature are shown as principal parameters in the prediction of microbubble behavior.

INTRODUCTION

Acoustic cavitation describes a phenomenon that involves growth and collapse of gas or vapor bubbles in a liquid under dynamic pressure. Acoustic waves produce such negative dynamic pressures because of their sinusoidal nature.

A single gas bubble trapped in a fluid through acoustic levitation can undergo radial or shape oscillations by varying standing-wave amplitude and frequency. In everyday experiences we encounter a diversity of multi-bubble systems in liquids. Furthermore, these two-phase systems can be generated in many ways such as, by mechanical, chemical, acoustic and optical excitations [1-3].

While engineers and physicists were developing the theoretical basis of bubble cavitation, its application in medical diagnostic began with the work of Gramiak [4]. In those early days only free-gas bubbles were used as contrast agents and its inherent shortcomings included indeterminate size, short life-time and inability for transverse lung circulation. Later, the fist-generation of contrast agents appeared, this generation distinguished five types of agents: free gas bubbles encapsulated gas bubbles, colloidal suspension, emulsions and aqueous solutions. Nowadays, contrast agents of the second and third generation are used; they are filled with gas of low solubility and coated by a phospholipid monolayer whose thickness is on the order of 2-4 nm [5]. The main feature of such agents is that they oscillate during sonication (the capacity to enhance the backscattered signal). These oscillations can result in linear backscattering at low acoustic pressure, nonlinear signals with harmonic frequencies at medium acoustic pressure, and microbubble disintegration at high acoustic pressure [6-7]. Microbubbles destruction by ultrasound has also raised questions about bio-effects in the vicinity of contrast agents.

Due to the aforementioned, countless resources has been invested in determining the dynamic behaviour of the ultrasonic contrast agents as well as single bubbles under specific conditions, trying to determine the main parameters and correlations involved on the stability, dynamics, and energy storage [7-10]. Furthermore, recent studies on the dynamics of bubbles include various fluids (highly viscous and viscoelastic) with different encapsulating materials (albumin, polymer, or lipid) in order to emulate body fluids [11-12]. However, these experimental proofs do not consider variations at initial conditions or the presence of other macroscopic structures that influence its stationary state and acoustic emissions.

In this work, we investigate the acoustic characteristics of encapsulated gas microbubbles and an air bubble in order to understand its radial dynamics under similar conditions. Light scattering is applied to measure the radial pulsations of individual/cloud microbubbles. The

acoustic emission waves are also acquired near the suspending microbubbles using a needle hydrophone. The waveforms are processed by means of Fourier and time-frequency analysis.

Mie scattering theory

One widely used method to determine the evolution of the bubble radius is Mie's scattering [10, 13]. The standard Mie technique consists of measuring the intensity of laser light scattered by a bubble. In the short wavelength limit [$l << R(t)$] the size of a homogeneous bubble is inferred from the fact that the scattering is proportional to $R^2(t)$. The scattered intensity depends on the dielectric constants of gas and the fluid at the bubble interface. The main parameter is the size parameter $\alpha = \pi d/\lambda$, where d is the scatter diameter and λ is the wavelength of the incident light. In SBSL applications, d changes continuously by over a factor of 10, and the intensity of scattered light changes by approximately a factor of 100 during the 30-μs acoustic cycle. This is in contrast to scattering from a solid sphere, in which the wavelength may be shifted a small quantity. The angular scattering pattern for a bubble is also different from that of a solid sphere.

Frequency and time-frequency theory

The formation and collapse of bubbles are nonlinear processes, and their behaviour is time-variant. The radial dynamics obtained by Mie scattering are waveforms that present changes of energy over time. The Fourier transform is employed for the estimation of the featured frequencies of the main processes to identify them as a function of frequency. Analysis in the frequency-domain of a signal $f(t)$ with finite duration is generally realized by means of the Fourier transform (FT). This analysis allows for the estimation of the energy contained in a range of frequencies. The corresponding amplitudes $|F(\omega)|$ are an average of the amplitudes present over the duration of the signal. Thus, the FT does not provide any evident information about the time of occurrence of these amplitudes. Nevertheless, the short-time Fourier transform (STFT) is basically the same FT but estimated for time-translated windows of the signal. These windows are represented by a compact-supported function $s(t)$. In this study a Hamming window is employed [14].

NOMENCLATURE

$R(t)$	[m]	Instantaneous radius of the bubble
R_0	[m]	Initial bubble radius
T	[^{0}C]	Temperature
P_0	[Pa]	Hydrostatic pressure in the liquid
P_v	[Pa]	Vapor pressure inside the bubble
$P(t)$	[Pa/s]	Driving acoustic pressure
Pa	[Pa]	Acoustic pressure
f	[Hz]	Driving frequency
$V(t)$	[V]	Voltage amplitude
Re	-	Reynolds number
De	-	Debora number
Special characters		
σ	[N/m]	Surface tension for the liquid-gas interface
$\sigma(R)$	[N/m]	Effective surface tension
η	[Pa s]	Dynamic viscosity of the liquid
κ	[Pa s]	Encapsulated viscosity
γ	[-]	Polytropic exponent of the gas
c	[m/s]	Sound velocity in the liquid
χ	[N/m]	Shell elastic modulus
Subscripts		
0		Initial value
f		Final value

EXPERIMENTAL APPARATUS

Sonoluminescence is emitted by a single air bubble that is levitated in an acoustic standing wave generated in a spherical flask filled with sterile water, (250 ± 3 mL). The sterile water is degassed for 5 min. The standing wave is excited by means of two hollow, cylindrical, piezoelectric transducers cemented to the outside of the flask (annular PZT C-5400, type I). A pill piezoelectric (MIC) is fixed to the outside of the flask to monitor the pressure field relative to the function generator output. The transducers are driven in the range of 30-70 kHz to a few volts amplitude with a function generator (with a preamplifier and an acoustic-amplifier of 500 W) through an inductive impedance-matching circuit. The drive frequency is adjusted to setup a radially symmetric standing wave in the flask. A small amount of air or diluted contrast agent is injected into the flask with a hypodermic syringe. A portion of the injected air or diluted agent contrast evolves into a single bubble levitated at the acoustic pressure antinode located at the center of the flask. With proper adjustment of the drive amplitude and frequency, this bubble reaches a state in which it undergoes cyclic, large-amplitude, radial oscillations, while it emits one pulse of SL per acoustic cycle when using gas bubble. When contrast agents are used, no luminescence is observed.

The experimental arrangement for generating sinusoidal acoustic field inside of a water-filled spherical resonator is shown in Figure 1.

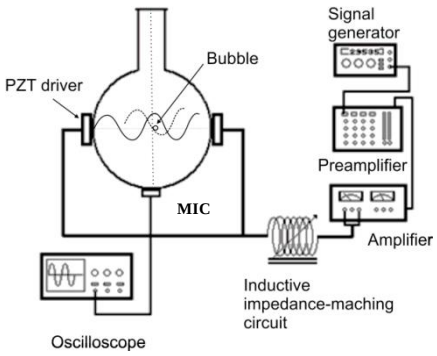

Figure 1 Experimental setup for generating a sinusoidal acoustic field inside of a spherical resonator indicating the main equipment

The experimental setup to apply the Mie scattering technique consists of: a continuous He-Ne laser (Research Electro-Optics, 12.0 mW, 633 nm, and 0.7 mm in diameter beam), a Hamamatsu photomultiplier tube module (PMT) with a red filter to detect only scattered laser light, and optical elements, see Figure 2.

The laser beam impinges on the bubble. The scattered light by the bubble is collected through a large angle, so that a large lens focuses the scattered light on to PMT. The PMT output, $V(t)$ is proportional to $R^2(t)$ plus the background level $\underline{V}(t)$. The noise level is measured by sending the laser light through the flask without the

bubble. The radius is then $\sqrt{V(t)}$-$\underline{V}(t)$, as plotted in Figure 4.

A PVDF needle-type hydrophone (Precision Acoustics Ltd.), 0.5 mm in diameter is placed inside the spherical flask in direct contact with the region of interest. The hydrophone, PMT and excitation output signals are recorded on a 1 GHz LeCroy LC584AM digital storage oscilloscope.

APPARATUS RESPONSE

The resonance frequency of the system and its harmonics are depicted in Figure 3. To find the spectrum in frequency, a sweep is performed by means of a function generator, and the local peaks are detected by measuring the voltage output in the MIC. Significantly, at higher resonance corresponds to a smaller size of trapped gas bubble.

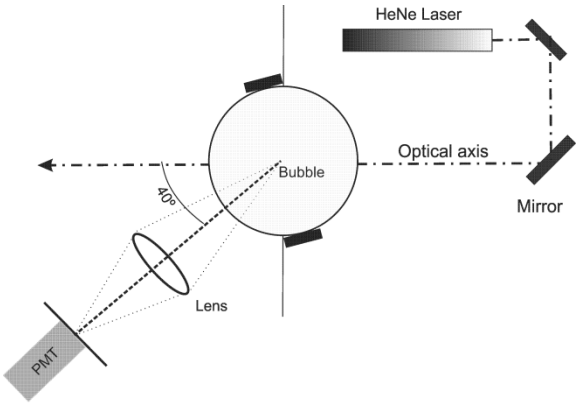

Figure 2 Experimental setup for Mie scattering measurements to obtain the radial oscillations of a sonoluminescence gas bubble

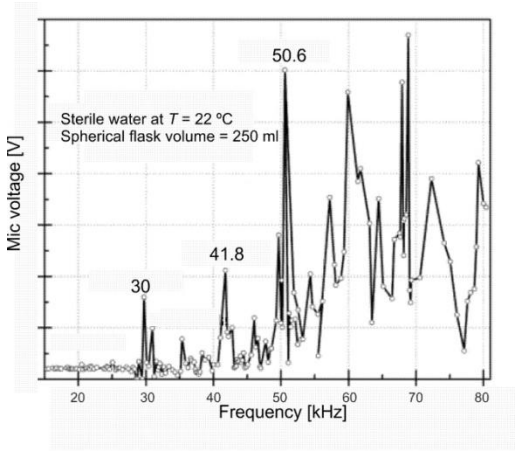

Figure 3 Frequency sweep of a spherical resonator filled with sterile water. The peaks correspond at local maxima where the occurrence of luminescence is probable.

MODELS

The experimental data of radial oscillations are corroborated using the Rayleigh-Plesset (**RP**) equation for a gas bubble. For encapsulated bubbles data, we use the linearized model of Marmottant *et al.* [15]; for this case, the shell features as surface dilatational viscosity K, surface tension σ (R) and elastic module χ are taken into account in the **RP** equation. Both models assume that: there is no heat or mass transfer through interface, the surrounding liquid is incompressible, the bubble wall velocity is no longer compared to sound speed of liquid ($\dot{R}(t) << c$), the bubble oscillation is only radial and never loses its spherical shape. Regarding the encapsulated bubble, the shell thickness must be less than the radius. These models describe nonlinear effects, such as during the compression phase associated with **SBSL,** and as encapsulated bubbles destroying effects. To solve this equations we apply a numerical procedure base on Runge-Kutta of 4th order. The initial parameter values as ρ, η, Pa, P_0, σ, γ, P_v, are displayed in table 1, and P_a= 1.6 MPa, P_0 =79.6 kPa.

Table 1. Initial parameter values of the **RP** equation

	Sterile water			PolySon H*	
ρ	998	[kg/m^3]	$\sigma(R_0)$	0.02	[N/m]
η	0.001	[Pa s]	K	6x10^{-9}	[Kg/s]
σ	0.07	[N/m]	χ	2.5	[N/m]
γ	1.07		R_o	3	[μm]

EXPERIMENTS

A series of experimental studies of the sinusoidal excitation method are carried out on air bubbles and encapsulated bubbles in degassed sterile water using the system described previously. The evolution of radial dynamic, as a function of time and temperature is followed with initial conditions of liquid at T_0 ~ 17 ºC. Then, the system evolves until it reaches room conditions, T_f ~ 22 ºC.

Air bubble

Figure 4 shows the radius-time curve for the air gas bubble showing oscillations over five acoustic cycles. The bubble was in luminescence conditions. The high pressure reached during the collapse produces the launch an outgoing spike, a shock wave, which is recorded by means a hydrophone, see Figure 5.

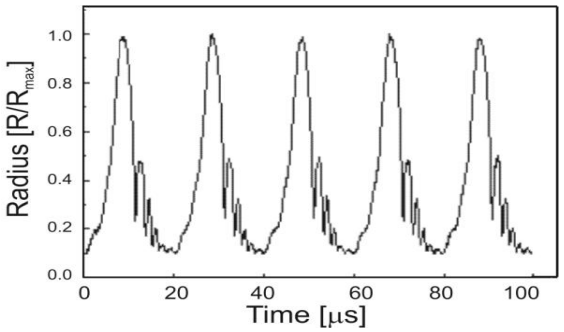

Figure 4 Instantaneous scattered intensity collected from a pulsating bubble radius

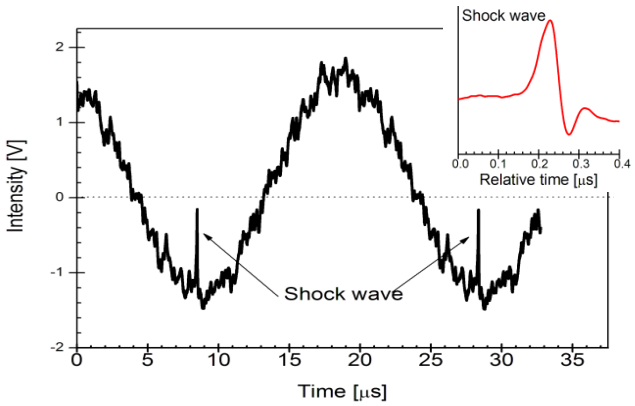

Figure 5 Driving ultrasonic field recorded by a hydrophone in which is clear the outgoing spikes produced by shock wave emission.

Figure 6 displays four inverted signals acquired with a PMT (the radii from laser light scattering). Note that the amplitude and number of afterbounces diminishing as a function of time. Radial dynamics in long time scale is not nonlinear anymore, as observed in the signal IV. The relaxation time for the bubble to return to its linear state was about 100 minutes with a temperature increase of 3.3 ºC.

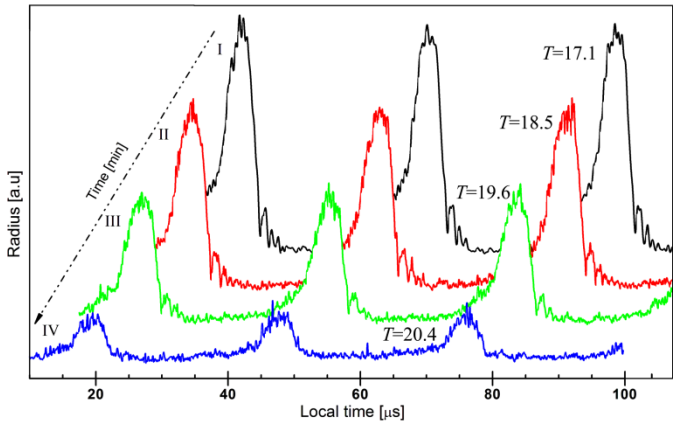

Figure 6 Waterfall plots of the inverted PMT signals as a function of longer times for a gas microbubble. I) Initial time, II) first 50 minutes, III) next 80 minutes, IV) then 104 minutes and finally disappears at 127 min. P_A = 1.6 ± 0.2M Pa, T_0 = 17ºC, and T_f = 23 ºC.

Ultrasound contrast agent / PolySon H

Figure 7 shows four inverted signals acquired by the PMT in which it is noted that after the compression phase almost no rebound occurs. Furthermore, the amplitude decreases more quickly, an order of magnitude smaller than in the gas bubble. Besides, this contrast agent presents tiny deformities due its polymeric shell. Its destruction under this acoustic field intensity is very quick. The relaxation time for this bubble to return to its linear state was about one minute with a temperature change of a tenth of a degree.

Figure 8 shows a comparison over one acoustic cycle for both microbubbles. The circles are experimental points, and solid lines are a simulation with the Rayleigh-Plesset equation. An important feature of the air bubble is that the amplitude of the afterbounces completely disappears before the beginning of the next cycle, which is not the case for the UAC bubble. At the acoustic pressure applied, both present an expansion phase longer than the contraction phase, but the first lobule of the UCA microbubble is more wide and with lower amplitude.

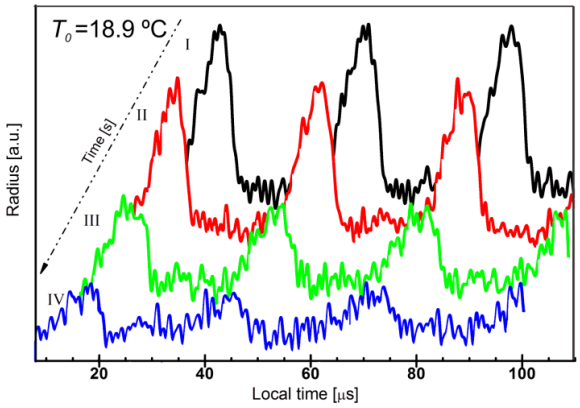

Figure 7 Waterfall plots of the inverted PMT signals as a function of longer times for a UCA microbubble. I) Initial time, II) first 12 s, III) next 24 s, IV) then 60 s, and finally disappears at 1.3 ± 0.5 min. T_0 = 18.9 ºC, and T_f = 19 ºC.

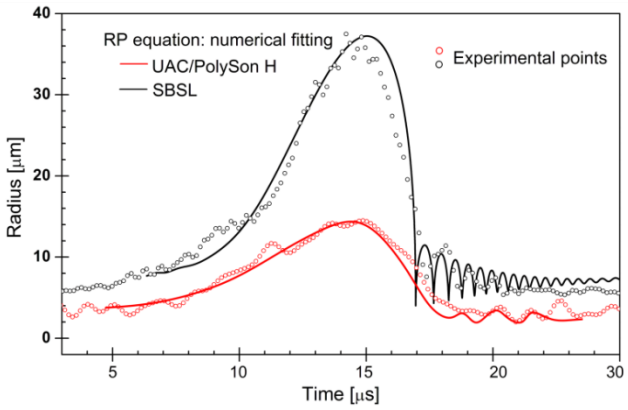

Figure 8 Comparison bubble dynamics with a full simulation with the Rayleigh-Plesset equation with uniform pressure (solid). The parameter were P_A = 1.6 ± 0.2 MPa, R_0= 6 μm f =35.12 kHz (black line), R_0 = 3 μm, f = 36.2 kHz (red line)

SPECTRAL ANALYSIS

Analysis of the acquired waveforms can reveal different phenomena, such as the shock wave emitted during the compression stage of luminescent gas bubble. Figure 8 shows a cycle for SBSL. Its radial oscillation show many peaks of high frequency, see the upper graph in Figure 9; its STFT revels a high peak near to the final compression stage and before the rebounding phase, in the range of 0.8 - 1.5 MHz which indicate a shock wave emission that corresponds with the time between 17-18 μs. For the UAC, radial oscillation shows wider peaks, see bottom image in Figure 9, its smooth STFT indicates a shock wave, and however its energy is almost constant reaching the 6 MHz frequency.

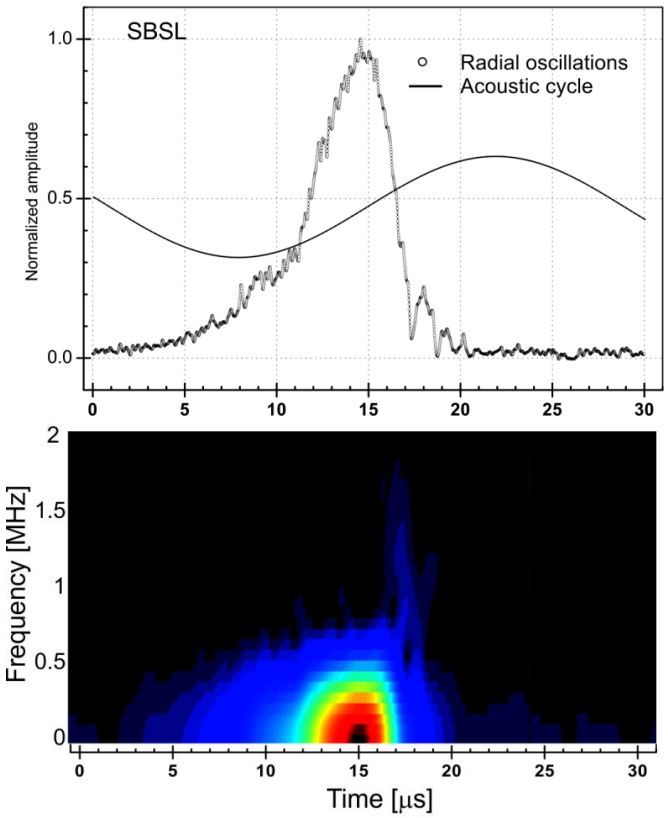

Figure 9 Radial dynamics from SBSL (upper graph) and its STFT bottom image).

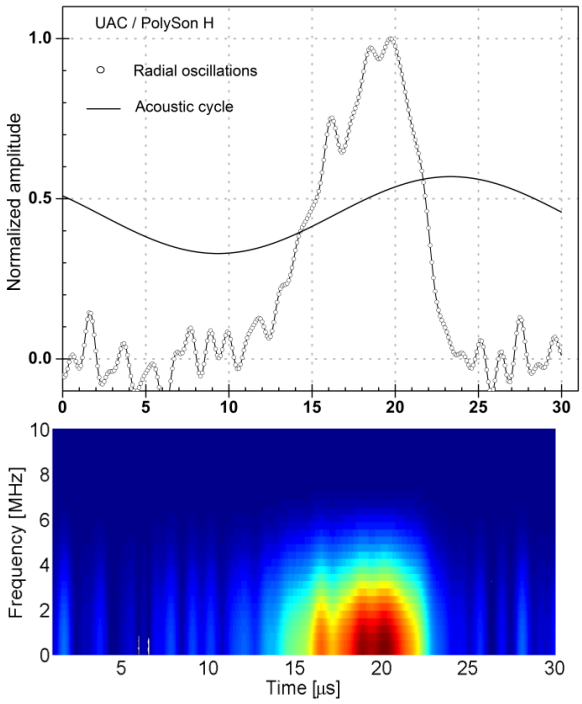

Figure 10 a) Radius–period plot of UAC microbubble, and their STFT

RESULTS

The dynamic behavior in both gas and UCA microbubbles under the same conditions (acoustic pressure 1.6 MPa, driven frequency 35-36 kHz, and initial temperature of liquid T_0 ~ 18º C) has the following differences in broad terms:

a) ***Oscillation***

To achieve asymmetric oscillation in both cases, it was necessary to increase the acoustic intensity for UCA microbubble a 33 %, see Figure 8.

Leaving each of the bubbles to oscillate freely, keeping constant all the parameters except for the liquid temperature, we find that the lifetime of the gas bubble is two orders of magnitude higher than the UCA microbubble, see Figures 6 and 7.

By applying a low-driven frequency, 35-36 kHz, the energy transferred to the bubbles in the expansion phase is large in time, so that the maximum radius achieved in gas bubble is one order of magnitude higher that in UCA microbubble. The rebound phase is almost indistinguishable in the behavior of the UCA microbubble, as observed in Figure 7.

b) ***Translation***

In short and long time regime, the air bubble almost does not present translational path, unlike an UCA bubble which does due to its short timeline.

c) ***Fragmentation***

The air bubble does not present an explosive fragmentation during the repetitive cycles, however the UCA microbubble develops a jet in which there is shell rupture and gas is released. Furthermore, sometimes the UCA microbubbles are aligned in the ultrasonic path between piezoelectric drivers; it is at this time when they undergo an explosive rupture of its shell with gas emission in jets form.

d) ***Shock wave***

The shock wave emission is clearly detected in the SBSL, as shown in Figure 5, and is also observable in the STFT of the oscillations waveforms, see Figure 9. Regarding the contrast agents, it is not possible to detect them with the same procedure, see Figure 10.

e) ***STFT analysis***

The STFT analysis of the radial oscillations waveforms for both types of bubbles indicates that:

1) **UCA bubble**: there is a larger shift between stress applied and strain reached, this is observed in Figure 8 in the slope of the curves during the expansion phase, due obviously to its shell; also its energy spectrum covers a broader bandwidth. There is not presence of shockwave at the onset of afterbounces, instead when the threshold

intensity of the driving pressure is reached; the bubble is destroyed with emission of a gas jet.

2) **Air bubble**: As the driving pressure increases, there is greater bubble expansion amplitude followed by rapid contractions and afterbounces. There are light emissions and a shockwave before the onset of rebounding. This is clear because there is no large difference in time between the applied stress and the resulting strain, due to its elastic gas-liquid interface. Its energy spectrum shows a narrow band indicating a strong energy concentration that is released as shock wave.

The above statements are in agreement with some references [5, 14-17].

f) ***Short and long regimen***

The Reynolds (*Re*) and Debora (*De*) numbers are dimensionless, used to characterize the fluid condition and fluidity of materials respectively. *Re*, is defined as the ratio of inertial to viscous forces; and $De = \lambda/T$, where T is a characteristic time for the deformation process and λ is the relaxation time. Considering the maximum radius reached and the time history waveforms for each bubble, we have:

Table 2 Air bubble versus UAC bubble

	Air bubble	UAC bubble
Re	8565±380	4312±210
De (Short regimen)	0.36±0.03	0.67±0.22
De (large regimen)	208	12

The above values indicate that, in general, the air bubble undergoes inertial collapse stronger than the UAC bubble. Considering a cycle (short regimen), both bubbles show a $De < 1$; indicating that both act viscoelastically. However in a long regimen, the air bubble is more elastic than the UAC bubble.

CONCLUSION

The dynamic behavior for two types of bubble (with and without shell) in short and long regimen has been developed. The examination of a single bubble has revealed that at a given temperature, the dynamic behavior is determined predominantly by the bubble diameter at rest and the intensity of the driving pressure. Furthermore, with respect to the UCA bubble, a small change of temperature drastically affects its dynamics. UAC bubbles are routinely used to obtain medical imaging and they do not represent a health risk. While this is true when the recommended acoustic intensity threshold is not exceeded, a slight change in temperature is enough to switch this threshold.

ACKNOWLEDGES

The authors gratefully acknowledge financial support from UNAM-DGAPA-PAPPIT under Grant IN 105212-3, IN 115712, II-FI-UNAM under Grant 1135 and 3130 from UNAM-II.

REFERENCES

[1] Ohl, C. D., Probing luminescence from nonspherical bubble collapse, *Phys. Fluids*, Vol. 14, 2000, pp. 2700-2708

[2] Harvey, E. N., Sonoluminescence and sonic chemiluminescence, *J. Am. Chem. Soc* , Vol. 61, 1939, pp. 2392–2398

[3] Khodorkovskii, M. A., Murashov, S. V., Artamonova, T. O, and Rakcheeva, L. P., Excitation of water molecules by electron impact with formation of OHº radicals in the A2 + state, *J. Phys. B: At. Mol. Opt. Phys.*, Vol. 42, 2009, pp. 215201-215206

[4] Gramiak R. and Shah P. M. Echocardiography of the aortic root, *Invest Radiol* Vol. 3, 1968, pp. 356-366

[5] Delale C. F. (Ed.) *Bubble Dynamics &Shock Waves*, Encapsulated Bubble Dynamics in Imaging and Therapy, Shock waves Vol. 8, 2013, pp. 259-289

[6] Calliada, F., Campani R., Botinelli O., Bozzini A., and Sommaruga M.G., Ultrasound contrasts agents basic principles, *European Journal of Radiology*, Vol. 27, 1998, pp. S157-S160

[7] Brotchie, A., Grieser, F., and Ashokkumar, M., Effects of power and frequency on bubble-size distributions in acoustic cavitation, *Phys. Rev. Lett.* Vol. 102, 2009, pp 084302-1-084302-4

[8] Yuang, C., Effects of acoustic insonations parameters on ultrasound contrast agent, *Ultrasound in Med & Biol*, Vol. 34, 2008, pp 1281-1291

[9] Chen, W.S., A comparison of the fragmentation thresholds and inertial cavitation doses of different ultrasound contrast agent, *J. Acoust. Soc. Am.*, Vol. 113, 2003, pp 643-651

[10] Barber, B. P., Hiller, R.A., Lofstedt, R., Putterman, S. J. and Weninger, K. R., Defining the unknown of sonoluminescence, *Phys. Rep.* Vol. 281, 1997, pp. 65-14.

[11] Jiménez, J., Bubble oscillation and inertial cavitation in viscoelastic fluids, *Ultrasonics*, Vol. 43, 2005, pp. 643-651

[12] Naude, J., Mendez, F., Non-linear oscillations of an elastic shell controlled by the interface pressure, *Mechanics Research Communications*, Vol. 37, 2010, pp. 673-677

[13] Lentz, W. J., Atchley A. A., and Gaitan D. F., Mie scattering from a sonoluminescing air bubble in water, *Appl. Opt.* Vol. 34, 1995, pp. 2648-2654

[14] Lathi B. P., *Signal Processing and Linear Systems*, Berkeley – Cambridge Press, Carmichael, CA, 1998

[15] Marmottan, P., van der Meer S., Emmer, M., and Versluis M., de Jong, N., Hilgenfeldt, S., and Lohse, D., A model for large amplitude oscillations of coated bubbles accounting for buckling and rupture, *J. Acoust. Soc. Am.*, Vol. 118, 2005, pp. 3499-3505

[16] Postema, M., Van Wamel, A., Lancée, C. T. and de Jong, N. Ultrasound-induced encapsulated microbubble phenomena, Ultrasound in Med. & Biol., Vol. 30, No. 6, 2004, pp. 827-840

[17] Mulvana, H., Stride, E., Tang, M., Hajnal, J. and Eckersley, R. Temperature-dependent differences in the nonlinear acoustic behavior of ultrasound contrast agents revealed by high-speed imaging and bulk acoustics, *Ultrasound in Med. & Biol*., Vol. 37, 9, 2011, pp 1509-1517